

INSTRUMENTS AND METHODS OF INVESTIGATION PACS numbers: 42.65.Re, 42.79.Jq

Uncertainty relation for modulated broadband laser pulses

K B Yushkov, V Ya Molchanov, E A Khazanov

DOI: https://doi.org/10.3367/UFNe.2020.06.038793

Contents

Abstract. The shaping of picosecond laser pulses with complicated amplitude and phase modulations is applied in various problems concerning the interaction of radiation with matter. Such pulses are generated by modulating femtosecond laser pulses with the help of programmable spectral filters with a complex transmission function based on spatial light modulators or acousto-optic dispersion delay lines. It is shown that the number of resolved elements and their contrast upon modulating chirped laser pulses satisfy the uncertainty relation, and the optimal bandwidth of the filter is twice the frequency range of the laser pulse. The results are experimentally confirmed for a femtosecond Ti:Sapphire laser with a high-resolution dispersion delay line.

Keywords: femtosecond laser pulse, pulse shaper, dispersion delay line, acousto-optic diffraction, uncertainty relation

1. Introduction

In 1946, D Gabor showed in his cardinal study, *Theory of Communications*, that the uncertainty relation between the minimal duration of a signal and its spectral width is one of the fundamental restrictions in the information theory [1]. It is well known that, due to this relation, a signal with spectral width Δf has the minimal rise time $\tau_r \approx 1/(2\Delta f)$ [2]. One of the directions of modern physics in which these relations play a decisive role is the optics of ultrashort laser pulses [3, 4].

Laser pulses with a complicated spatiotemporal shape are used in various problems related to the interaction of radiation with matter. Among the most urgent issues are laser inertial fusion [5–7], electron beam shaping with the help of photocathodes [8, 9], and the generation of tunable terahertz radiation [10, 11]. The modulation of nanosecond laser radiation can be performed by electro-optic modulators with a time resolution of about 100 ps [12]. The modulation of broadband ultrashort laser pulses is achieved by more sophisticated methods, such as spectral modulation and spectral synthesis [13]. Spectral modulation is based on the phase-and-amplitude modulation of a laser pulse, while spectral synthesis uses the coherent combining of laser beams with different spectra and different pulse shapes.

In this paper, we consider the more often encountered first case, namely, the problem of obtaining a specified shape of the amplitude envelope and the specified phase modulation of a single chirped laser pulse with the help of a programmable pulse shaper.

The duration of an ultrashort laser pulse is determined by its spectral width and phase modulation. The problem of laser pulse shaping for pulses with arbitrary shapes can be formulated in terms of the theory of signal processing: how to synthesize a frequency filter with a complex transmission function providing a specified envelope shape and signal phase. The principal feature of the problem under study is the use of phase-modulated signals for which the product of their duration on the spectral width greatly exceeds the Gabor limit. The types of modulation depend on practical applications. In fast-ignition laser fusion problems, for example, the formation of the required pulse intensity envelope is the most important one [5, 6]; however, the use of a complicated pulse shape or additional phase modulation ensures a decrease in the level of undesirable stimulated Raman scattering [7, 14]. Another example is the synthesis of terahertz wave packets, which can be performed using femtosecond lasers in two ways: either by purely phase modulation [10, 15, 16] or phase-and-amplitude modulation [11] of laser pulses.

At present, two widespread methods exist to control the shape of broadband laser pulses: using spatial modulators based on liquid crystals, more rarely spatial acousto-optic (AO) noncollinear modulators, or with the help of extended AO interaction in crystals. In the first case, additionally, an optical system for converting a temporal spectrum into a spatial one with a diffraction grating, a spatial spectrum

K B Yushkov [1, a], **V Ya Molchanov** [1, b], **E A Khazanov** [2, c]
[1] National University of Science and Technology MISIS, Leninskii prosp. 4, 119049 Moscow, Russian Federation
[2] Institute of Applied Physics, Russian Academy of Sciences, ul. Ul'yanova 46, 603950 Nizhny Novgorod, Russian Federation
E-mail: [a] konstantin.yushkov@misis.ru, [b] aocenter@misis.ru, [c] khazanov@appl.sci-nnov.ru

Received 6 June 2020
Uspekhi Fizicheskikh Nauk **191** (8) 874 – 881 (2021)
Translated by M Sapozhnikov

modulation with a spatial light modulator, and then the inverse conversion of the spatial spectrum into the temporal one are used [17–22]. Such an optical scheme is often called a '4F-shaper' because of the use of a double optical Fourier system with antiparallel gratings introducing zero dispersion [4].

Another type of programmable shaper is based on the AO interaction in distributed ultrasonic Bragg gratings with arbitrary phase-and-amplitude modulation [23–28]. In a AO birefringent crystal, an ultrasonic wave is synthesized, which irs an inhomogeneous volume phase grating with different phase-matching regions located along the laser beam propagation direction. Such devices are called AO dispersion delay lines, the transmission function of the device being complex. In dispersion lines, as a rule, the quasi-collinear geometry of the anisotropic AO interaction is used, which changes the polarization of light, for example, from an ordinary (O) wave to an extraordinary (E) wave [29]. The difference between the velocities of the O and E waves in a crystal allows one to obtain either the positive or negative group-velocity dispersion. Pulses with a fixed shape can be produced using static volume Bragg gratings created in a bulk light guide or an optical fiber by the photorefractive method or the nonlinear modification of a material by focused femtosecond laser pulses [30, 31]. The interaction of plane waves in the AO and photorefractive Bragg gratings is described by similar coupled-wave equations [32].

Irrespective of the type of shaper, it has a finite frequency bandwidth

$$B_\omega = \omega_{\max} - \omega_{\min}\,, \tag{1}$$

where $\omega_{\min}$ and $\omega_{\max}$ are the lower and higher frequencies, respectively, transmitted by the shaper. Thus, the problem is how to reproduce the most accurately a laser pulse with the specified envelope shape $A(t)$ and phase modulation with the help of an optoelectronic device with a finite transmission band. The equivalent formulation of the problem in the spectral representation consists in the determination of the amplitude $|\widetilde{S}(\omega)|$ and phase $\Phi(\omega) = \arg \widetilde{S}(\omega)$ of the spectrum restricted by the band B_ω which most accurately correspond to the signal $A(t)$. If the input radiation spectrum $\widetilde{S}_{\text{in}}(\omega)$ is known and nonzero in the interval $[\omega_{\min}, \omega_{\max}]$, the problem is reduced to the determination of the transmission function

$$\widetilde{H}(\omega) = \frac{\widetilde{S}(\omega)}{\widetilde{S}_{\text{in}}(\omega)} \tag{2}$$

of a linear filter. The specified shape $A(t)$ of a signal with a finite duration cannot be formed absolutely accurately with such a filter because its spectrum is infinite and is *a priori* broader than the filter bandpass B_ω. To estimate the accuracy, criteria are needed that are significant from the point of view of applications. Such criteria may be the rise and decay times of modulation fronts, contrast, the maximum number of resolved elements, and the transmission coefficient.

2. Optimal passband of a filter

Consider an arbitrary electromagnetic-wave pulse with the electric field strength $E(t)$ specified in a finite time interval $t \in [0, T_0]$. Let us represent the pulse in the complex form $E(t) = A(t) \exp[\mathrm{i}\phi(t)]$. Now, we will take an interval with duration τ so small that the pulse amplitude $A(t)$ can be assumed to change linearly in it and the carrier frequency ω_c can be assumed constant (Fig. 1a). Then, the field strength in this interval with duration τ is

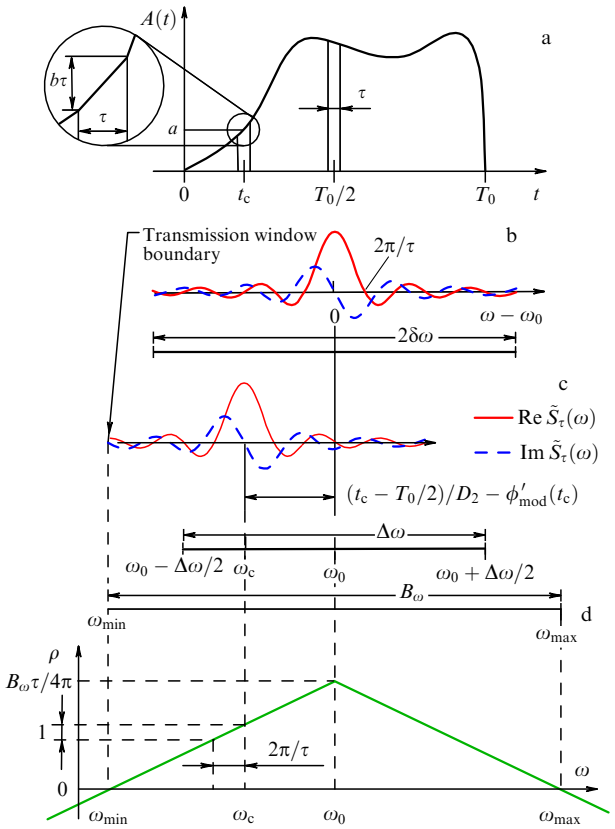

Figure 1. Representation of an arbitrary pulse shape in the form of a sequence of elementary trapezium-like signals (a); corresponding components of the spectrum (b) for the central elementary signal $t_c = T_0/2$ and (c) the elementary signal shifted to the boundary of the interval $[0, T_0]$; (d) dimensionless parameter of the shift of spectral components of a chirped pulse.

$$E_\tau(t) = \left[a + b(t - t_c)\right] \operatorname{rect} \frac{t - t_c}{\tau} \exp(\mathrm{i}\omega_c t)\,, \tag{3}$$

where a and b are coefficients describing the mean value and the derivative of the envelope, respectively, rect is the unit rectangular window function, and t_c is the center position of the time window. We will represent the initial pulse shape $E(t)$ as a superposition of trapezium-like functions (3) with different t_c and ω_c. Assuming that envelope $A(t)$ is nonnegative, we obtain the following restriction on coefficients a and b:

$$a \geqslant 0\,, \qquad |b| \leqslant \frac{2a}{\tau}\,. \tag{4}$$

The elementary trapezium-like pulse (3) has the spectrum $\widetilde{E}_\tau(\omega) = \exp(-\mathrm{i}\omega t_c)\widetilde{S}_\tau(\omega - \omega_c)$ with the low-frequency component having the real part

$$\operatorname{Re} \widetilde{S}_\tau(\omega) = a\tau \operatorname{sinc} \frac{\omega\tau}{2} \tag{5}$$

and the imaginary part

$$\operatorname{Im} \widetilde{S}_\tau(\omega) = \frac{b\tau^2}{2} \operatorname{sinc}' \frac{\omega\tau}{2}\,, \tag{6}$$

where the prime denotes the derivative of the function.

The expansion of the pulse envelope into elementary trapezium-like pulses (3) and spectral components corresponding to them on the frequency scale are shown in Fig. 1; the high-frequency part of spectral components determined by the factor $\exp(\mathrm{i}\omega t_\mathrm{c})$ is not shown. The full width at half-maximum of the central maximum of the function $|\widetilde{S}_\tau(\omega)|^2$ depends on b and changes from $1.77\pi/\tau$ for $b=0$ (a rectangular pulse with a constant amplitude in the interval) up to $2.21\pi/\tau$ for $|b|=2a/\tau$ (the amplitude in the interval changes to zero and the trapezium transforms into a triangle).

The value of $|S_\tau(\omega)|$ tends to zero with infinitely increasing frequency. As a result, this value becomes lower than the noise level in a shaper for some detuning from the central frequency, the so-called cutoff frequency $\delta\omega$. The noise threshold depends on both technical factors, the finite resolution of digital-to-analog electronic converters being the most important, and physical factors determined first of all by the scattering of light in the optical path of the shaper. For example, in an AO dispersion delay line, the noise level in a diffracted beam is considerably determined by the anisotropy of acoustic properties and the AO crystal growth defects, the ultrasound excitation system, and thermal gradients in the AO interaction region. We can assume that for each elementary pulse $E_\tau(t)$, only the components of the spectrum $\widetilde{S}_\tau(\omega)$ whose detuning does not exceed the cutoff frequency $\delta\omega$ are nonzero (Fig. 1b). These components satisfy the inequality

$$|\omega-\omega_\mathrm{c}|<\delta\omega\,. \tag{7}$$

If the shaper band is broad enough, i.e., $B_\omega>2\delta\omega$, then the distortions of the elementary pulse $E_\tau(t)$ in the central part of the spectrum are determined only by the noise limit in the system. Spectral components lying below cutoff frequency $\delta\omega$ at the edges of the spectrum are lost (Fig. 1c), resulting in additional distortions in the shape of the elementary trapezium-like pulse. Thus, the influence of the boundaries of the shaper bandpass on distortions has a threshold nature related to cutoff frequency $\delta\omega$.

Consider a linearly chirped laser pulse $E(t)$ of duration T_0 with phase

$$\phi(t)=\omega_0 t+\frac{\Delta\omega}{2T_0}\left(t-\frac{T_0}{2}\right)^2+\phi_\mathrm{mod}(t)\,, \tag{8}$$

where $\phi_\mathrm{mod}(t)$ is an arbitrary phase modulation and ω_0 and $\Delta\omega$ are the central frequency and the characteristic width of the spectrum, respectively. The carrier frequency of an elementary trapezium-like pulse at the time moment t_c is

$$\omega_\mathrm{c}=\omega_0-\frac{t_\mathrm{c}-T_0/2}{D_2}+\phi'_\mathrm{mod}(t_\mathrm{c})\,, \tag{9}$$

where $D_2\approx -T_0/\Delta\omega$ is the second-order dispersion defined as the second frequency derivative of the spectral phase $\Phi(\omega)=\arg\widetilde{S}(\omega)$ of signal $E(t)$ [4]. The quadratic phase modulation in a chirped laser pulse $A(t)$ shifts the carrier frequency ω_c of the elementary pulse and the low-frequency envelope $\widetilde{S}_\tau(\omega)$ of its spectrum to the red if $t_\mathrm{c}<T_0/2$ (Fig. 1c), and to the blue if $t_\mathrm{c}>T_0$. The additional shift of the carrier frequency can be caused by phase modulation $\phi_\mathrm{mod}(t)$.

The position of the pulse spectrum $\widetilde{S}_\tau(\omega)$ with respect to the boundaries of the interval $[\omega_\mathrm{min},\omega_\mathrm{max}]$ can be described by

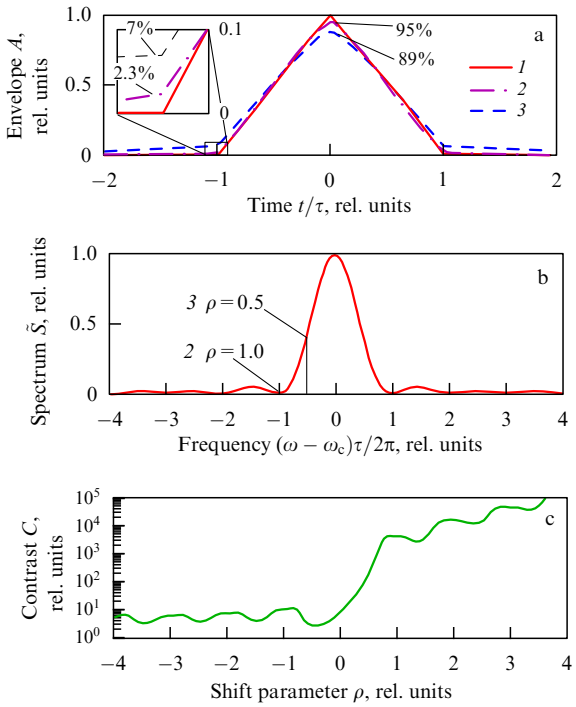

Figure 2. Distortions of a single triangular pulse with shift ρ caused by the asymmetric transmission of spectral components: (a) envelope shape; (b) pulse spectrum; (c) contrast of a pulse with a distorted spectrum. *1* — initial pulse shape; *2* — envelope shape for $\rho=1$; *3* — envelope shape for $\rho=0.5$.

the dimensionless shift parameter (Fig. 1d),

$$\rho=\frac{\tau}{2\pi}\left(\frac{B_\omega}{2}-|\omega_\mathrm{c}-\omega_0|\right). \tag{10}$$

The normalization factor is chosen so that the central maximum of spectrum (5) corresponds to $\rho=1$. The maximum value $\rho=B_\omega\tau/4\pi$ is reached at the interval center for $\omega_\mathrm{c}=\omega_0$, which corresponds to the case in Fig. 1b. At the interval boundaries, $\rho=0$, while outside the interval, the shift parameter takes negative values.

Spectral components corresponding to different temporal parts of a pulse being formed are located asymmetrically with respect to the frequency band $[\omega_\mathrm{min},\omega_\mathrm{max}]$ of the shaper. The transmission asymmetry will affect most strongly the pulse components $E_\tau(t)$ located near the boundaries of the interval $[0,T_0]$, when the interval between the edge of the transmission window of the shaper and frequency ω_c is of the order of $2\pi/\tau$, i.e., is close to the characteristic width of the function $|\widetilde{S}_\tau(\omega)|^2$. To reproduce correctly a specified shape of pulse $E(t)$ in the entire interval $[0,T_0]$, the shaper passband $[\omega_\mathrm{min},\omega_\mathrm{max}]$ should be wider than the variation range $[\omega_0-\Delta\omega/2,\omega_0+\Delta\omega/2]$ of the carrier frequency of radiation.

To answer the question of how much the width B_ω of the transmission window should exceed the width $\Delta\omega$ of the spectrum, it is necessary to consider the modulation contrast. A quantitative example might be a single pulse with the minimal duration 2τ with a triangular envelope. Such a pulse, shown in Fig. 2a, is a superposition of two successive trapezium-like pulses (3), each with duration τ and envelope derivatives $b=\pm 2a/\tau$. Its spectrum (Fig. 2b) is described by the expression

$$\widetilde{S}(\omega)=\mathrm{sinc}^2\,\frac{(\omega-\omega_\mathrm{c})\tau}{2}\,. \tag{11}$$

Near the boundary of the transmission range $[\omega_{\min}, \omega_{\max}]$, some of the spectral components come outside the range. In this case, the pulse shape is distorted: its amplitude decreases and a nonzero pedestal appears for $|t| \geqslant \tau$, whose influence on the contrast is decisive (Fig. 2a).

Depending on applications, the definition of the contrast can be different. For example, measurements of the spectral resolution using the method of frequency-contrast characteristics in the optics of ultrashort laser pulses involve periodic modulation, and contrast is measured by the ratio of the maximum and minimum intensities in the adjacent spectral regions [33]. The contrast for a triangular pulse is defined as the ratio of the maximum radiation intensity in the pulse for $|t| \leqslant \tau$ to the maximum intensity of the pedestal for $|t| > \tau$.

As mentioned above, the asymmetric position of the spectrum with respect to the boundaries of the range $[\omega_{\min}, \omega_{\max}]$ results in a decrease in contrast. The calculated contrast of a triangular pulse is presented in Fig. 2. Calculations were performed assuming that spectral components are lost only on one side corresponding to the nearest boundary of the transmission window of the shaper.

Theoretically, the contrast $C(\rho)$ increases infinitely as parameter ρ increases. However, the physical contrast is always restricted by a control device. As a rule, the maximum contrast for a single pulse does not exceed $10^3 - 10^4$. In the case of periodic pulse modulation, the contrast is reduced due to the overlap of functions $\widetilde{S}(\omega)$ corresponding to adjacent pulses. In this case, the main characteristic of the resolution is the modulation transfer function [33].

By comparing (7) and (10), we can conclude that the contrast for pulse components satisfying the inequality

$$2\pi\rho > \delta\omega\tau \tag{12}$$

will be determined only by the cutoff frequency $\delta\omega$, while the contrast for components with the carrier frequency lying near the transmission-window boundary of the shaper at a distance smaller than $\delta\omega$ will decrease. To provide the same conditions for the reproduction of pulse $A(t)$ in the entire interval $[0, T_0]$, condition (12) should be fulfilled in particular at the edges of the spectrum, i.e., for $\omega_c = \omega_0 \pm \Delta\omega/2$. Then, we obtain from (10) the width τ of the elementary interval

$$\tau = \frac{4\pi\rho}{B_\omega - \Delta\omega}\,, \tag{13}$$

while the number $N = T_0/\tau$ of resolvable elements in the envelope shape of a chirped laser pulse can be represented, taking (9) into account, as a function of the laser radiation bandwidth $\Delta\omega$,

$$N = \frac{D_2\Delta\omega(B_\omega - \Delta\omega)}{4\pi\rho}\,. \tag{14}$$

The transmission range B_ω here is a parameter. The maximum of N is reached for

$$\Delta\omega = \frac{B_\omega}{2}\,. \tag{15}$$

Taking this into account, expression (14) can be written as the inequality

$$N\rho \leqslant \frac{D_2 B_\omega^2}{16\pi}\,. \tag{16}$$

Expression (16) represents an *uncertainty relation* in the sense that an increase in the number of resolvable elements reduces the contrast and vice versa. The equality in (16) is fulfilled only for the optimal ratio (15) of the radiation spectrum width $\Delta\omega$ and the transmission window B_ω.

Let us explain how the optimal ratio (15) between quantities $\Delta\omega$ and B_ω is obtained. We will assume that a shaper has a constant number M of resolvable spectral channels (elements) in the frequency bandwidth B_ω. Then, spectral band $\Delta\omega$ of the chirped laser pulse contains $M_1 = M\Delta\omega/B_\omega$ channels. If the transmission bandwidth B_ω of the shaper is increased, the spectral contrast increases due to the increase in the cutoff frequency $\delta\omega = 2\pi\rho/\tau$, but the number M_1 of resolvable channels per frequency range $\Delta\omega$ decreases. Because of linear frequency modulation (9), the number of resolved channels is equal to the number N of time-resolved pulses in the envelope $A(t)$ of the chirped laser pulse. On the contrary, as the frequency range B_ω of the shaper is reduced to the lower boundary $B_\omega = \Delta\omega$, the number of spectral channels increases to the maximum value $M_1 = M$, but the value of ρ decreases. Correspondingly, the contrast of channels forming the edges of the laser radiation spectrum decreases and, therefore, the number of resolved channels with a fixed contrast satisfying condition (12) decreases.

Thus, we can conclude that the optimal bandwidth B_ω of the shaper should be twice the laser spectral width $\Delta\omega$, this ratio being independent of requirements for the modulation contrast. In this case, modulation contrast $C(\rho)$ determines in fact the number N of resolvable positions in the pulse shape according to (16). We will now consider the application of this principle to shapers with different architectures.

3. Architecture of laser pulse shapers and control-signal shaping

The two types of common shapers differ in the principle of their action on laser radiation [4]. In 4F-shapers, the modulation is performed in a spectral region, i.e., a spatial modulator directly specifies the amplitude and phase of each spectral component. In extended Bragg gratings, the modulation is performed in a temporal region, i.e., different spectral components are delayed with respect to each other, and their amplitudes are simultaneously controlled. In this case, the profile of an inhomogeneous Bragg grating is related to its spectral transmission function $\widetilde{H}(\omega)$ by the Fourier transform. Let us consider both types of shapers in more detail.

3.1 4F-shaper based on a spatial modulator

The time shaping of laser pulses with the help of a spatial modulator is performed using the setup shown in Fig. 3. It consists of a diffraction grating, a Fourier lens, one or several spatial modulators, and an output system containing a Fourier lens and a diffraction grating. Most commonly used are spatial modulators based on liquid crystals. Despite the high spatial resolution of modern liquid-crystal matrices, one of their disadvantages is the pixel structure, producing side distortions of signals such as phase–amplitude couplings, the appearance of sideband maxima, and Gibbs oscillations [8, 9, 34, 35]. An alternative to liquid crystals is AO modulators without the pixel structure operating in the same optical Fourier system [20–22].

The spectral transmission window of a 4F-shaper is determined by the angular dispersion of the grating and the

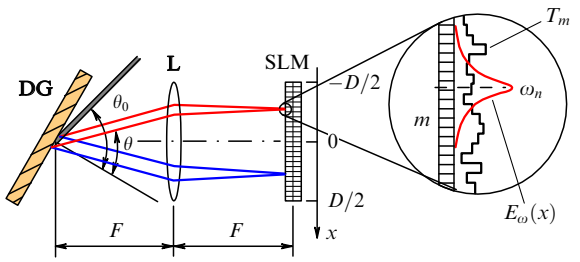

Figure 3. Physical model of a 4F-shaper takes into account the finite size of a focal spot in the Fourier plane of an optical system and the discrete structure of a liquid-crystal spatial modulator: DG (diffraction grating); L (lens); SLM (spatial light modulator). Output optical system consisting of a Fourier lens and a diffraction grating located symmetrically to the right of the modulator is not shown.

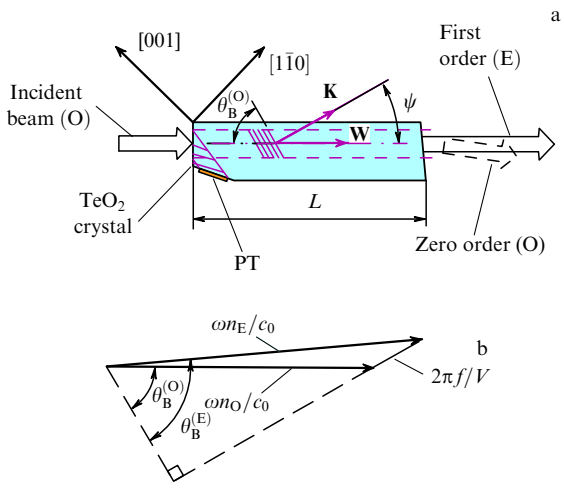

Figure 4. Quasi-collinear geometry of the AO interaction in a paratellurite crystal: (a) schematic of the AO dispersion delay line. PT — piezoelectric transducer; (b) diagram of wave vectors.

modulator aperture D:

$$B_\omega \approx \frac{D}{F}\left(\frac{\mathrm{d}\theta}{\mathrm{d}\omega}\bigg|_{\omega_0}\right)^{-1} = \frac{\omega_0^2 D}{2\pi c_0 \mu F}\sqrt{1-\left(\sin\theta_0 - \frac{2\pi c_0 \mu}{\omega_0}\right)^2}, \tag{17}$$

where F is the focal distance of a lens, θ_0 and θ are the angles of incidence and diffraction from the grating, respectively, μ is the groove density of the grating, and c_0 is the speed of light in a vacuum. Note that expression (17) is approximate, because it ignores the nonlinearity of the dependence $\theta(\omega)$. The width of the transmission window of the shaper can be changed by using lenses with different focal distances F or diffraction gratings with different groove density μ, and also by changing the angle of radiation incidence θ_0 on the grating.

The physical model of a 4F-shaper takes into account the finite size of a focal spot in the Fourier plane, which can overlap several pixels of the spatial light modulator [4, 13]. The transmission coefficients T_m of pixels can be found from the system of equations

$$\sum_{m=1}^{M} T_m P_{mn} = \mathrm{FT}\left\{A(t)\exp\left[\mathrm{i}\phi_{\mathrm{mod}}(t)\right]\exp\left[\mathrm{i}\,\frac{\Delta\omega}{2T_0}(t-t_0)^2\right]\right\}_{\omega_n}, \tag{18}$$

where quantities P_{mn} characterize the overlap of the mth pixel of the matrix with the focal spot of the spectral component of radiation at the carrier frequency $\omega = \omega_n$ and

$$t_0 = \left(\frac{1}{2} - \frac{\omega_0}{\Delta\omega}\right)T_0\,. \tag{19}$$

In the general case, coefficients T_m are complex, i.e., they provide both the amplitude and phase modulation, which can be achieved by using two sequentially located liquid-crystal spatial modulators or one AO spatial modulator.

3.2 Acousto-optic dispersion delay line

Unlike a 4F-shaper based on a spatial modulator, Bragg gratings do not require additional optical elements. The transmission bandwidth B_ω of an AO grating is determined exclusively by the radio-frequency band of a control radio signal. The maximum bandwidth is restricted by matching the electric impedance of a piezoelectric transducer and reaches an octave [36]. For AO dispersion delay lines, a narrower impedance matching band can be used, which provides the linear phase characteristic of an ultrasonic wave in a crystal [37]. Note here that the broadening of the transmission band B_ω results in a proportional increase in the control power of a radio-frequency (RF) signal applied to a piezoelectric transducer if the constant diffraction efficiency is maintained. To increase the efficiency, spectral resolution and group-velocity dispersion, AO crystals with a large interaction length are used [38]. The quadratic phase modulation (chirping) of a RF signal reduces the peal amplitude of the ultrasound [39]. The frequency range Δf of the ultrasound is uniquely determined by the Bragg phase matching condition and is proportional to the spectral width $\Delta\omega$ of optical radiation.

Quasi-collinear diffraction in paratellurite (TeO_2) single crystals was first proposed and experimentally demonstrated in [40]. The typical geometry of the quasi-collinear AO interaction used in dispersion delay lines is shown in Fig. 4. A similar geometry can also be used in other AO crystals. However, for smaller walk-off angles ψ (between the ultrasound wave vector **K** and the Umov vector **W**), the reflection geometry of elastic waves will be different [41]. A shear acoustic wave excited by a piezoelectric transducer is reflected from the input optical face of the crystal, the angle of incidence of an acoustic beam being selected so that the Umov vector **W** of the reflected acoustic beam is collinear to the optical beam. Note that the structure of acoustic beams in strongly anisotropic crystals is essentially asymmetric, while their diffraction divergence can exceed by many times the divergence in an isotropic medium [42]. For this reason, dashed lines in Fig. 4a do not represent the real boundaries of the acoustic beam. The phase matching condition for AO diffraction in a birefringent crystal is determined by the propagation direction of an acoustic wave specifying the velocity V and the walk-off angle ψ, by the mutual orientation of optical and acoustic waves specified by the Bragg angle θ_B, and by the dispersion of the refractive index of an AO crystal: $n_O(\omega)$ and $n_E(\omega)$. A diagram of wave vectors (Fig. 4b) allows the dependence $\omega_B(f)$ to be found in the implicit form

$$f = \frac{\omega_B V}{2\pi c_0}\left|n_E(\omega_B)\sin\theta_B^{(E)} - \sqrt{n_O^2(\omega_B) - n_E^2(\omega_B)\cos^2\theta_B^{(E)}}\right|, \tag{20}$$

where Bragg angles are related by the expression $n_O \cos\theta_B^{(O)} = n_E \cos\theta_B^{(E)}$, and the Bragg angle for an ordinary wave is $\theta_B^{(O)} = \pi/2 - \psi$ in the quasi-collinear geometry of diffraction [29].

The synthesis of an ultrasonic Bragg grating is an inverse problem to that considered in Section 2: along the propagation path of a laser beam, it is necessary to form the one-dimensional distribution of the refractive index providing the specified complex transmission function $\widetilde{H}(\omega)$ in the spectral interval $[\omega_{min}, \omega_{max}]$. This problem is reduced to the calculation of the amplitude and phase modulation functions of the RF wave packet $U(t)$ with the finite duration $T_a = L\cos\psi/V$ applied to a piezoelectric transducer to excite an ultrasonic wave in the AO crystal. The quantity T_a is the maximum possible duration of an ultrasonic wave packet in a crystal of a specified size. In other words, unlike Section 3.1, the problem is considered for an elastic rather than an electromagnetic wave, and time and frequency are interchanged. If the effective duration of the ultrasonic signal $T_s \leqslant T_a$ is specified, the RF signal can be calculated as

$$U(t) = \mathrm{FT}^{-1}\left\{\widetilde{H}\big(\omega_B(f)\big)\exp\left[\mathrm{i}\,\frac{\pi T_s}{\Delta f}(f-f_0)^2\right]\right\}, \qquad (21)$$

where the operator FT^{-1} performs the inverse Fourier transform with integration over the variable $2\pi f$. The quantity T_s determines the duration of the central maximum of the function $|U(t)|$ [39]. In practice, the signal $U(t)$ is calculated using functions of discrete variables f and t and the algorithm of fast Fourier transform and reproduced with a digital waveform generator [43].

Conclusions made in Section 2 about the relation between the variation range $\Delta\omega$ of the carrier frequency of an optical pulse and the transmission window B_ω of the shaper are completely valid for the duration of radio-frequency wave packets with the only difference being time changed to frequency. The width B_ω of the transmission window corresponds to the full duration T_a of the wave packet, and the spectral width $\Delta\omega$ corresponds to the effective signal duration T_s. In this case, expression (21) for the RF signal amplitude $U(t)$ is similar in its structure to expression (18) for the spectral transmission coefficient $T(\omega)$ of a spatial modulator: the required quantity is determined by the direct or inverse Fourier transform of the specified function multiplied by a quadratic phase factor. In this case, phase matching condition (20) establishes a one-to-one correspondence between the radio-frequency band Δf and the spectral width $\Delta\omega$ of a laser pulse. Thus, by specifying the transmission window width $B_\omega = 2\Delta\omega$ and the corresponding frequency variation $2\Delta f$ during the full signal duration T_a, we obtain

$$T_s = 0.5T_a\,, \qquad (22)$$

which is similar to condition (15) for spectra. The fulfillment of relation (22) provides the maximum contrast of modulation of laser radiation by an AO dispersion delay line in the entire spectrum interval $[\omega_{min}, \omega_{max}]$.

4. Experimental study of modulation by the acousto-optic method

Experiments were performed using a Ti-sapphire laser setup. The experimental setup is presented in Fig. 5. The original AO

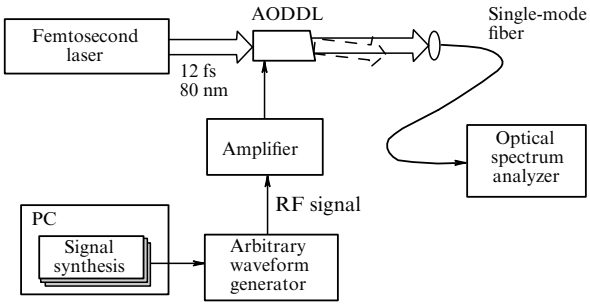

Figure 5. Experimental setup.

dispersion delay line based on a paratellurite (TeO_2) crystal [38] used in experiments provided the instrumental function width of 0.24 nm at the central wavelength of 790 nm of the femtosecond laser. The time aperture was chosen as $T_a = 51.2$ μs. The width of the emission spectrum at 795 nm was 80 nm, corresponding to $\Delta\omega = 0.24$ fs^{-1}, and the ultrasonic frequency range $\Delta f = 9.6$ MHz.

The resolution and modulation depth of a shaper were measured by the method of modulation transfer function [33]. The method is based on the periodic modulation of a spectrum and measurements of the contrast between the maxima and minima of the transmission function. Note that periodically modulated pulses are also required for laser drivers for photocathodes [8].

In the first series of experiments, an ultrasonic grating filled the entire aperture of the crystal, i.e., $T_s = T_a$. This case corresponds to the choice of the shaper bandwidth without a margin with respect to the width of the spectrum $B_\omega = \Delta\omega$. In the second series of experiments, condition (22) was fulfilled, which corresponds to the optimal relation for spectra (15). The results of measurements of diffracted emission spectra are presented in Fig. 6. The periodic modulation of the spectrum was specified in the form of a meander with a period of 0.96 nm, corresponding to the number of independent points $N = 167$. The modulation depth was measured with respect to the reference spectrum, which was the output emission spectrum of the AO dispersion line with the rectangular transmission window.

The first series of experiments (Figs 6a, b) was performed for the nonoptimal band $B_\omega = \Delta\omega$. One can see that the spectrum of diffracted emission exhibits a considerable (more than 5 dB) decrease in the modulation depth at its edges. Note that the contrast decrease obviously has a threshold nature for the critical shift $\rho = \delta\omega\tau/2\pi$ (see (12)). The corresponding transition region in the spectrum is shown in Fig. 6b on an enlarged scale. For the given experimental parameters, these spectral regions represent about 30% of the full width of the spectrum $\Delta\omega$. The smaller the modulation period, the higher the cutoff frequency $\delta\omega$ and, correspondingly, a decrease in the modulation depth is observed in a broader region at the edges of the spectrum.

The results of the second experimental series shown in Figs 6c, d correspond to the optimal width of the transmission window (15) and (22): $B_\omega = 2\Delta\omega$ and $T_s = 0.5T_a = 25.6$ μs. It can be seen that no decrease in the modulation depth is observed at the edges of the spectrum. In this case, a considerable part of the RF signal energy (in our case, about 10%) corresponds to intervals $[0, T_a/4]$ and $[3T_a/4, T_a]$. The absence of particularly these components in the signal spectrum upon AO interaction reduces the modulation

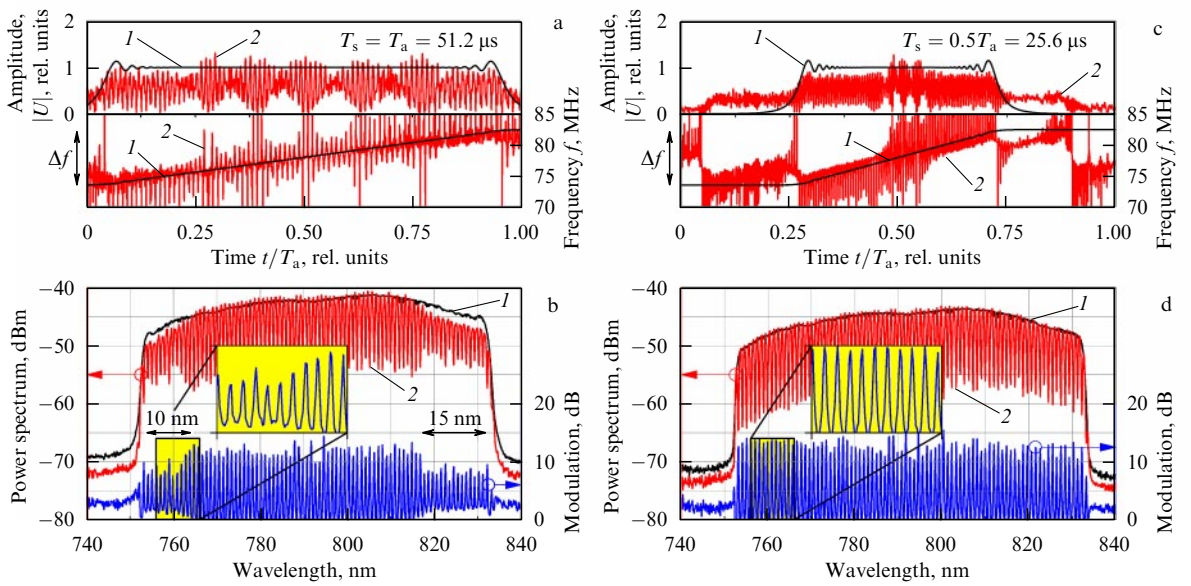

Figure 6. Envelope $|U(t)|$ and instant frequency $f(t)$ of a control RF signal (a, c), power spectrum and contrast of femtosecond laser radiation (b, d) upon modulation with an AO shaper; (a, b) total transmission window equal to the spectrum width, $B_\omega = \Delta\omega$; (c, d) total transmission window equal to twice the spectrum width, $B_\omega = 2\Delta\omega$. *1* — reference ultrasonic signal and corresponding power spectrum of diffracted radiation without modulation; *2* — ultrasonic signal and power spectrum of laser radiation modulated with a period of 0.96 nm. Insets show the contrast in the transient region at an enlarged scale.

contrast at the edges of the optical spectrum (Figs 6a, b). A further increase in B_ω did not improve the contrast of laser radiation, in accordance with uncertainty relation (16), because the number M_1 of resolvable spectral channels in the interval $\Delta\omega$ decreased.

5. Conclusions

We have shown that, upon formation of a chirped laser pulse with an arbitrary envelope shape by a programmable spectral filter with a finite transmission band, the number N of resolvable elements and the modulation contrast C are restricted by the uncertainty relation. The maximum of the product of the number of resolvable elements by the contrast is achieved if and only if the total transmission band B_ω of a programmable filter is twice the spectral width $\Delta\omega$ of the chirped pulse. For any other relation between the values of B_ω and $\Delta\omega$, either a decrease in the number of resolvable elements or a decrease in the contrast at the edges of the chirped laser pulse is observed. These conclusions have been demonstrated experimentally with the AO dispersion delay line used as a shaper of femtosecond laser pulses.

Acknowledgments. K Yushkov and V Molchanov thank the Russian Science Foundation (project no. 20-12-00348).

References

1. Gabor D *J. Inst. Electr. Eng. Pt. III Radio Commun. Eng.* **93** 429 (1946)
2. Max J *Méthodes et Techniques de Traitment du Signal et Applications aux Mesures Physiques* (Paris: Masson, 1981); Translated into Russian: *Metody i Tekhnika Obrabotki Signalov pri Fizicheskikh Izmereniyakh* (Moscow: Mir, 1983)
3. Akhmanov S A, Vysloukh V A, Chirkin A S *Optics of Femtosecond Laser Pulses* (New York: American Institute of Physics, 1992); Translated from Russian: *Optika Femtosekundnykh Lazernykh Impul'sov* (Moscow: Nauka, 1988)
4. Weiner A M *Ultrafast Optics* (New York: Wiley, 2009)
5. Gus'kov S Yu *Plasma Phys. Rep.* **39** 1 (2013); *Fiz. Plazmy* **39** 3 (2013)
6. Atzeni S et al. *New J. Phys.* **15** 045004 (2013)
7. Bel'kov S A et al. *Plasma Phys. Control. Fusion* **61** 025011 (2019)
8. Mironov S Yu et al. *Phys. Usp.* **60** 1039 (2017); *Usp. Fiz. Nauk* **187** 1121 (2017)
9. Kuzmin I et al. *Laser Phys. Lett.* **16** 015001 (2019)
10. Ahn J et al. *Opt. Express* **11** 2486 (2003)
11. Ovchinnikov A V et al. *Quantum Electron.* **46** 1149 (2016); *Kvantovaya Elektron.* **46** 1149 (2016)
12. Burkhart S C et al. *Proc. SPIE* **2633** 48 (1995)
13. Weiner A M *Rev. Sci. Instrum.* **71** 1929 (2000)
14. Albright B J, Yin L, Afeyan B *Phys. Rev. Lett.* **113** 045002 (2014)
15. Yushkov K B et al. *Phys. Rev. A* **96** 043866 (2017)
16. Yushkov K B, Molchanov V Ya *IEEE J. Sel. Top. Quantum Electron.* **26** 8700108 (2020)
17. Mazurenko Yu T *Opt. Spectrosc.* **57** 357 (1984); *Opt. Spektrosk.* **57** 583 (1984)
18. Weiner A M, Heritage J P, Kirschner E M *J. Opt. Soc. Am. B* **5** 1563 (1988)
19. Gu C et al. *Opt. Lett.* **40** 4018 (2015)
20. Dugan M A, Tull J X, Warren W S *J. Opt. Soc. Am. B* **14** 2348 (1997)
21. Ghosh A et al. *Opt. Lett.* **41** 524 (2016)
22. Dinda S, Bandyopadhyay S N, Goswami D *OSA Continuum* **2** 1386 (2019)
23. Pozhar V E, Pustovoit V I *Sov. J. Quantum Electron.* **17** 509 (1987); *Kvantovaya Elektron.* **14** 811 (1987)
24. Fermann M E et al. *Opt. Lett.* **18** 1505 (1993)
25. Verluise F et al. *J. Opt. Soc. Am. B* **17** 138 (2000)
26. Gao L, Herriot S I, Wagner K H *IEEE J. Sel. Top. Quantum Electron.* **12** 315 (2006)
27. Molchanov V Ya et al. *Appl. Opt.* **48** C118 (2009)
28. Molchanov V Ya et al. *Teoriya i Praktika Sovremennoi Akustooptiki* (Theory and Practice of Modern Acousto-Optics) (Moscow: MISiS, 2015)
29. Molchanov V Ya, Voloshinov V B, Makarov O Yu *Quantum Electron.* **39** 353 (2009); *Kvantovaya Elektron.* **39** 353 (2009)
30. Glebov L B et al. *Opt. Eng.* **53** 051514 (2014)
31. Antipov S et al. *Opt. Express* **24** 30 (2016)
32. Yariv A, Yeh P *Optical Waves in Crystals* (New York: Wiley, 1984); Translated into Russian: *Opticheskie Volny v Kristallakh* (Moscow: Mir, 1987)

33. Yushkov K B, Molchanov V Ya *Opt. Lett.* **38** 3578 (2013)
34. Dorrer C, Salin F *IEEE J. Sel. Top. Quantum Electron.* **4** 342 (1998)
35. Pestov D, Lozovoy V V, Dantus M *Opt. Express* **17** 14351 (2009)
36. Molchanov V Ya, Makarov O Yu *Opt. Eng.* **38** 1127 (1999)
37. Yushkov K B et al. *IEEE Trans. Ultrason. Ferroelectr. Freq. Control* **67** 1040 (2020)
38. Didenko N V et al. *Quantum Electron.* **45** 1101 (2015); *Kvantovaya Elektron.* **45** 1101 (2015)
39. Molchanov V Ya, Yushkov K B *Opt. Express* **22** 15668 (2014)
40. Voloshinov V B et al. *Sov. Tech. Phys. Lett.* **18** (2) 33 (1992); *Pis'ma Zh. Tekh. Fiz.* **18** (2) 33 (1992)
41. Molchanov V Ya, Chizhikov S I, Makarov O Yu, in *Acoustics'08 Paris* (Paris: Société Français d'Acoustique, 2008) p. 827
42. Mantsevich S N et al. *Ultrasonics* **78** 175 (2017)
43. Yushkov K B, Makarov O Yu, Molchanov V Ya *Opt. Lett.* **44** 1500 (2019)